Mean-Field Dynamics of Spin-Orbit Coupled Bose-Einstein Condensates

Yongping Zhang, Li Mao, and Chuanwei Zhang

Mean-field Dynamics of Spin-Orbit Coupled Bose-Einstein Condensates

Yongping Zhang, Li Mao, and Chuanwei Zhang*

Department of Physics and Astronomy, Washington State University, Pullman, WA, 99164 USA

Spin-orbit coupling (SOC), the interaction between the spin and momentum of a quantum particle, is crucial for many important condensed matter phenomena. The recent experimental realization of SOC in neutral bosonic cold atoms provides a new and ideal platform for investigating spin-orbit coupled quantum many-body physics. In this Letter, we derive a generic Gross-Pitaevskii equation as the starting point for the study of many-body dynamics in spin-orbit coupled Bose-Einstein condensates. We show that different laser setups for realizing the same SOC may lead to different mean field dynamics. Various ground state phases (stripe, phase separation, etc.) of the condensate are found in different parameter regions. A new oscillation period induced by the SOC, similar to the Zitterbewegung oscillation, is found in the center of mass motion of the condensate.

Spin-orbit coupling (SOC) for electrons plays a crucial role in many important condensed matter phenomena and applications, such as anomalous and spin Hall effects [1], topological insulator [2], spintronic devices [3], *etc.* However, the observation of SOC physics in nature solid state systems are often hindered by the unavoidable disorder and impurities. In this context, ultra-cold atomic gases provide an ideal platform for exploring novel SOC physics and device applications, owing to their unprecedented level of control and precision in experiments. In ultra-cold atomic gases, SOC can be generated through the laser-atom interaction, which yields Abelian or non-Abelian gauge fields for atoms in the dressed state basis [4–6]. The recent broad interest in spin-orbit coupled cold atoms is mainly motivated by their remarkable applications [4–20], ranging from the observation of Majorana fermions and the associated non-Abelian quantum statistics [12, 16], the design of atomtronics/spintronics devices [8, 9, 21], to the generation of magnetic monopoles [4], *etc.* An important difference between electrons and cold atoms is that, while electrons are fermions, ultra-cold atoms may be bosons, leading to novel spin-orbit physics that has not been explored in solids.

A benchmark experiment along this research direction is the recent realization of the one-dimensional (1D) SOC for cold bosonic atoms [15], which brings a completely new avenue for the study of the many-body dynamics of spin-orbit-coupled Bose-Einstein condensates (SOC-BECs). It is well-known that the starting point for the investigation of many-body dynamics of a BEC is the mean-field Gross-Pitaevskii (G-P) equation [22], whose general formula is still lacked for the SOC-BEC. In this Letter, we derive a generic G-P equation for the SOC-BEC and investigate their ground states and collective excitations. Our main results are:

(i) We find that the mean field dynamics depend on not only the SOC itself, but also the method to generate it because the effective pseudospin states in different laser setups for the realization of the same SOC can be different superpositions of atom hyperfine states with different s-wave scattering lengths. This fact is now taken into account in the mean-field interaction terms in the pseudospin space in the G-P equation. We find that the mean-field interaction energy may depend not only on the density, but also the phase of the condensate (*i.e.*, terms like $\Psi_1^2 \Psi_2^{*2} + c.c.$), which, to the best of our knowledge, have not been explored in previous literature [18–20]. We show that the phase dependent mean field terms can emerge for one type of laser setup (denoted as a complex system), but vanish for another (denoted as a simple system), with both laser setups implementing the same Rashba SOC.

(ii) We analyze the condensate wavefunctions for both systems in various parameter regions. In the strong interaction and SOC region, there exist two distinct phases for the condensate density: Thomas-Fermi (TF) and stripe. While in the weak and medium interaction or SOC region, spatial separation between two pseudospin components is observed.

(iii) The low energy collective excitations in spin-orbit coupled BECs are investigated, for the first time, through the center-of-mass (COM) motion of the condensate when a sudden shift of the center of the harmonic trap is applied. We find a novel, shift direction and distance dependent, oscillation frequency in the COM motion induced by the SOC, similar as the Zitterbewegung (ZB) oscillation in the free space [9]. However, the new oscillation period is linearly proportional to the SOC strength (in contrast to the inverse proportion in the ZB oscillation [9]). It is also independent on the atom interaction strength. Both oscillation period and amplitude are different for the simple and complex systems, even though they share the same physical parameters.

Consider ultra-cold bosonic atoms confined in a quasi-two-dimensional (xy plane) harmonic trap with a tripod electronic level scheme (Fig. 1a). The atom dynamics along the $\hat{\mathbf{z}}$ direction are frozen by a deep optical trap or lattice. The hyperfine ground states $|1\rangle$, $|2\rangle$, $|3\rangle$ are coupled with the excited state $|0\rangle$ using three blue-detuned lasers with the Rabi frequencies Ω_1, Ω_2, and
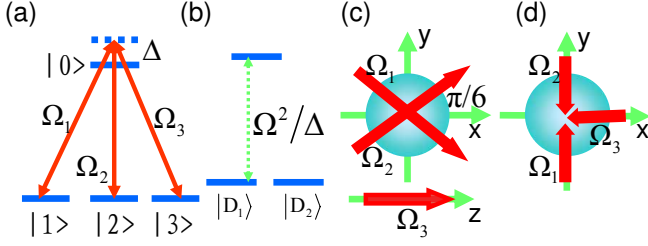
Figure 1: (Color online) A tripod scheme for implementing Rashba spin-orbit coupling. (a) The atom-laser coupling. (b) The lowest three energy levels composed of hyperfine ground states $|1\rangle$, $|2\rangle$, $|3\rangle$. $|D_1\rangle$ and $|D_2\rangle$ are degenerate dark states. $\Omega = \sqrt{|\Omega_1^2| + |\Omega_2^2| + |\Omega_3^2|}$. (c,d) Two different laser configurations [8, 16] for the tripod scheme.

Ω_3. The Hamiltonian of the system can be written as $H = \sum_i H_s(\mathbf{r}_i) + H_{int}$ with the single particle Hamiltonian

$$H_s(\mathbf{r}) = \mathbf{p}^2/2m + V(\mathbf{r}) + H_I(\mathbf{r}), \qquad (1)$$

where $V(\mathbf{r}) = m\left(\omega_\perp^2 r^2 + \omega_z^2 z^2\right)/2$ is the harmonic trapping potential with the corresponding trapping frequencies ω_z and $\omega_\perp$. $H_I(\mathbf{r}) = -\hbar\Delta|0\rangle\langle 0| - \hbar\left(\Omega_1|0\rangle\langle 1| + \Omega_2|0\rangle\langle 2| + \Omega_3|0\rangle\langle 3| + H.c.\right)$ describes the atom-laser interaction, and Δ is the detuning to the state $|0\rangle$. The diagonalization of the Hamiltonian $H_I(\mathbf{r})$ yields two degenerate darks states $|D_1\rangle = \sum_{\alpha=1}^{3} d_\alpha(\mathbf{r})|\alpha\rangle$, $|D_2\rangle = \sum_{\alpha=1}^{3} f_\alpha(\mathbf{r})|\alpha\rangle$ and two bright states (Fig. 1b), where the coefficients $d_\alpha(\mathbf{r})$, $f_\alpha(\mathbf{r})$ are determined by the laser parameters Ω_i and Δ [23]. In experiments, a large detuning Δ is chosen to suppress the spontaneous emission of photons that heats the atom gas. The blue-detuned lasers are used to ensure the degenerate dark states are the ground states of the system to avoid the collision loss. In the subspace spanned by the pseudospin states $|\uparrow\rangle \equiv |D_1\rangle$ and $|\downarrow\rangle \equiv |D_2\rangle$,

$$H_s(\mathbf{r}) = \mathbf{p}^2/2m + \gamma(p_x\sigma_y - p_y\sigma_x) + V(\mathbf{r}), \qquad (2)$$

where γ, the Rashba SOC strength, is equal to $\hbar k/2\sqrt{3}m$ and $(\sqrt{2}-1)\hbar k/m$ for the two laser setups shown in Figs. 1c and 1d, respectively. k is the wavevector of the lasers. The s-wave scattering interaction between atoms can be written as $H_{int} = \sum_{i<j}\sum_{\alpha,\beta=1}^{3} g_{\alpha\beta}\delta(\mathbf{r}_i^\alpha - \mathbf{r}_j^\beta)|\alpha\rangle_i|\beta\rangle_j\langle\alpha|_i\langle\beta|_j$, where $\mathbf{r}_i^\alpha$ is the position of the atom i in the hyperfine state $|\alpha\rangle_i$, $g_{\alpha\beta} = 4\pi\hbar^2 a_{\alpha\beta}/m$, $a_{\alpha\beta}$ is the s-wave scattering length between atoms in the hyperfine states $|\alpha\rangle$ and $|\beta\rangle$.

In the Hartree approximation, the many-body wavefunction of the bosonic system can be taken as the product of the single-particle wave function $|\Psi(\mathbf{r}_1, \mathbf{r}_2, \ldots, \mathbf{r}_N)\rangle = \prod_{i=1}^{N}|\Phi(\mathbf{r}_i)\rangle$, where $|\Phi(\mathbf{r})\rangle = \Phi_\uparrow(\mathbf{r})|D_1(\mathbf{r})\rangle + \Phi_\downarrow(\mathbf{r})|D_2(\mathbf{r})\rangle$ with the normalization condition $\int d\mathbf{r}(|\Phi_\uparrow(\mathbf{r})|^2 + |\Phi_\downarrow(\mathbf{r})|^2) = 1$. The G-P equation

can be obtained through the standard minimization of the mean-field energy functional $E(\Phi_\uparrow, \Phi_\downarrow) = \langle\Psi|H|\Psi\rangle$ with respect to $\Phi_\uparrow^*$ and $\Phi_\downarrow^*$ [22]. Because the scattering length is between atoms in different hyperfine states, the interaction energy $\langle\Psi|H_{int}|\Psi\rangle$ should be evaluated within the hyperfine state basis, $i.e.$, $|\Phi(\mathbf{r})\rangle = \sum_{\alpha=1}^{3}[\Phi_\uparrow(\mathbf{r})d_\alpha(\mathbf{r}) + \Phi_\downarrow(\mathbf{r})f_\alpha(\mathbf{r})]|\alpha\rangle$. With a straightforward calculation for such energy functional minimization, we derive the G-P equation for a SOC-BEC

$$i\hbar\partial\Phi/\partial t = H_s\Phi + \Gamma\Phi. \qquad (3)$$

Here the two component wavefunction $\Phi = (\Phi_\uparrow, \Phi_\downarrow)^T$ in the pseudospin basis $\{|\uparrow\rangle, |\downarrow\rangle\}$. The nonlinear term $\Gamma = \begin{pmatrix}\Gamma_1 & \Gamma_2 \\ \Gamma_2^* & \Gamma_3\end{pmatrix}$, where $\Gamma_1 = C_1|\Phi_\uparrow|^2 + C_2|\Phi_\downarrow|^2 + 2\text{Re}(C_3\Phi_\uparrow^*\Phi_\downarrow)$, $\Gamma_2 = C_3|\Phi_\uparrow|^2 + C_4|\Phi_\downarrow|^2 + C_5\Phi_\uparrow^*\Phi_\downarrow$, and $\Gamma_3 = C_2|\Phi_\uparrow|^2 + C_6|\Phi_\downarrow|^2 + 2\text{Re}(C_4\Phi_\uparrow^*\Phi_\downarrow)$ [24]. C_3, C_4 and C_5 terms, which are absent in previous study, originate from the linear superposition of hyperfine states for a pseudospin state. We see that not only the density, but also the relative phase between two components, play an important role on the dynamics of the BEC. Although our derivation for the mean-field interaction terms is based on the tripod schemes illustrated in Fig. 1, it also applies to other schemes for generating Rashba SOC using more hyperfine states (e.g. [25]).

For simplicity, we assume $g_{\alpha\beta} = g_1$ for $\alpha \neq \beta$ and $g_{\alpha\beta} = g_0$ for $\alpha = \beta$ with the corresponding scattering lengths a_1 and a_0. However the nonlinear G-P equation (3) works for any $g_{\alpha\beta}$. C_i depend strongly on the laser configurations for implementing the Rashba SOC. Here we consider two laser setups for the tripod level scheme (Fig. 1a) that have been investigated previously in the literature [8, 16, 23]. In the first setup (Fig. 1c), we have the SOC strength $\gamma = k\sqrt{\hbar/12m\omega_\perp}$, $C_3 = C_4 = C_5 = 0$, $C_1 = C_6 = \chi(2a_0 + 4a_1)/3$, and $C_2 = \chi(4a_0 + 2a_1)/3$ (the simple system) with $\chi = 2N\sqrt{2\pi m\omega_z/\hbar}$. Here we rescale the G-P equation (3) with the energy, time and length units $\hbar\omega_\perp$, $\omega_\perp^{-1}$, and $\sqrt{\hbar/m\omega_\perp}$ respectively. The unit for γ is a velocity $\sqrt{\hbar\omega_\perp/m}$. In the second setup (Fig. 1d), $\gamma = (\sqrt{2}-1)k\sqrt{\hbar/m\omega_\perp}$, $C_1 = C_6 = \chi[(12-8\sqrt{2})a_0 + (8\sqrt{2}-10)a_1]$, $C_2 = \chi[(24-16\sqrt{2})a_0 + (16\sqrt{2}-22)a_1]$, $C_3 = C_4 = -i\chi(7\sqrt{2}-10)(a_0 - a_1)$, and $C_5 = \chi(4\sqrt{2}-6)(a_0 - a_1)$ (the complex system).

We numerically solve the G-P equation (3) using the imaginary time evolution method and obtain the ground state of the condensate. In the simple system, there are two different types of phases in the region of strong SOC ($\gamma \gg 1$) and interaction ($C_i \gg 1$): the Thomas-Fermi (TF) phase (Fig. 2a) when $C_1 \geq C_2$ (equivalent to $a_1 \geq a_0$) and the stripe phase when $C_1 < C_2$ (Fig. 2c) [18]. In the TF phase, the maximum densities of two components locate at the harmonic trap center, but the phase of the condensate varies like a plane wave $\exp(i\mathbf{k}\cdot\mathbf{r})$ (Fig. 2b). In the stripe phase, the density for
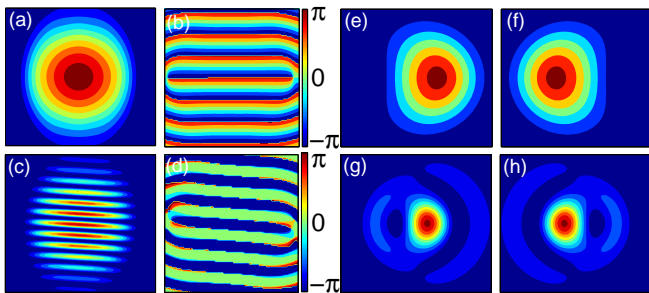
Figure 2: (Color online) Condensate wavefunction Φ in the simple system. (a,b) Density $|\Phi_\uparrow|^2$ (a) and phase $\arg(\Phi_\uparrow)$ (b) in the TF phase. $C_1 = 10$, $C_2 = 6$, $\gamma = 10$. (c,d) In the stripe phase. $C_1 = 6$, $C_2 = 10$, $\gamma = 10$. (e,f) Density $|\Phi_\uparrow|^2$ and $|\Phi_\downarrow|^2$ with $C_1 = 10, C_2 = 6$, $\gamma = 1$. (g,h) Density $|\Phi_\uparrow|^2$ and $|\Phi_\downarrow|^2$ with $C_1 = C_2 = 0, \gamma = 10$.

each pseudospin component forms a set of stripes (Fig. 2c) and two components are spatially separated. There is a sharp change of the condensate phase in and outside the stripe region (Fig. 2d). The total density of two components has a TF distribution for both phases. The direction of the condensate phase variation $\nabla \arg(\Phi_\sigma)$ is spontaneously selected, along which the density distribution is wider. We find that the density profile in each hyperfine state has the same structure (TF or stripe) as that in the pseudospin state, therefore the TF and stripe phases should be observable by directly measuring the density in each hyperfine state.

In the medium SOC region ($\gamma \sim 1$), there exists spatial separation between the atom densities of two pseudospin components when $C_1 \geq C_2$ (Figs. 2e, 2f). The separation can be understood from the spin-dependent force $\mathbf{F} = \frac{d\mathbf{p}}{dt} = 2\gamma^2(\mathbf{k} \times \hat{e}_z)\sigma_z$ generated by the Rashba SOC, where $\mathbf{k}$ is the momentum of atoms and along the condensate phase variation direction. $\mathbf{F}$ has the opposite directions for two pseudospins and is along the $\hat{\mathbf{x}}$ direction when the phase variation is along the $\hat{\mathbf{y}}$ direction (Fig. 2b), leading to the spatial separation of two pseudospin components along the $\hat{\mathbf{x}}$ direction (Figs. 2e, 2f). The separation due to the spin-dependent force is more transparent in the non-interacting region (Figs. 2g, 2h) without involving the complexity from the interaction. However, the separation between two components decreases not only for very strong SOC ($\gamma \gg 1$, Fig. 2a), but also for very weak SOC ($\gamma \ll 1$), which can be understood based on $\mathbf{F} \propto \gamma^2$ and the zero separation for a regular spinor BEC without SOC.

In the complex system, similar TF and stripe phases also exist in the strong SOC and interaction region. However, significant differences between the simple and complex systems exist for the low energy collective excitations even though their condensate phases are similar. Here we consider the COM motion of the condensate subject to a sudden shift of the center of the harmonic

trap. It is well-known that the COM motion of a BEC without SOC is a dipole oscillation whose frequency is the harmonic trap frequency and does not depend on the nonlinearity [26]. On the other hand, the interference between two Rashba spin-orbit energy bands yields the ZB oscillation [9] for a single particle in the free space with the oscillation period inversely proportional to γ^2. In this Letter, we study the COM motion of a BEC in the presence of interaction, a harmonic trap, and Rashba SOC.

The COM motion

$$\langle \mathbf{r}(t) \rangle = \int (|\Phi_\uparrow(\mathbf{r}, t)|^2 + |\Phi_\downarrow(\mathbf{r}, t)|^2) \mathbf{r} d\mathbf{r} \qquad (4)$$

of the condensate can be obtained by numerically solving the G-P equation (3) and is plotted in Figs. 3a and 3b (Figs. 3c, 3d) for the TF phase in the simple (complex) system. In the simple system, when the shift of the center of the harmonic trap D is along the $\hat{\mathbf{x}}$ direction (perpendicular to the condensate phase variation $\nabla \arg(\Phi_\uparrow)$ direction $\hat{\mathbf{y}}$), the COM motion along the $\hat{\mathbf{x}}$ direction is perfectly periodic with two periods (Fig. 3a): one corresponds to the harmonic trap frequency, the other is much larger and linearly proportional to the SOC strength γ (Fig. 4). The COM motion along the $\hat{\mathbf{y}}$ direction is similar. However, when the shift of the harmonic trap is along the $\hat{\mathbf{y}}$ direction, the COM motion along the $\hat{\mathbf{y}}$ direction possesses only the harmonic trap frequency and the oscillation amplitude is strongly damped (Fig. 3b). The COM motion along the $\hat{\mathbf{x}}$ direction vanishes.

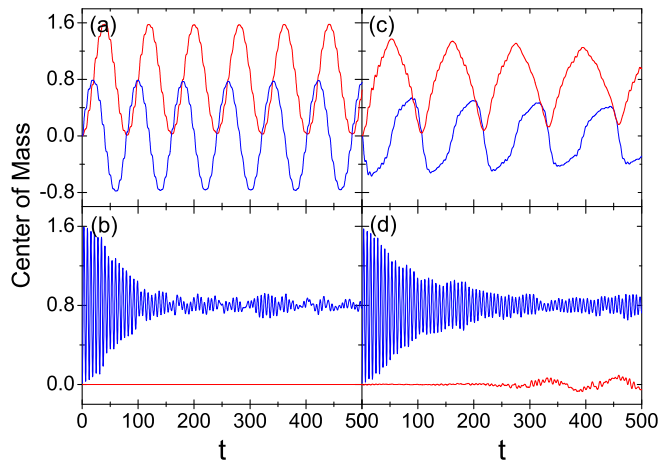The different COM motions along different shifting di-

Figure 3: (Color online) The center of mass motion. Red lines: $\langle x \rangle$; Blue lines: $\langle y \rangle$. (a,b) The simple system with the corresponding condensate wavefunction in Figs. 2a and 2b. The shift of the center of the harmonic trap $D = 0.8$. The shifts are along the $\hat{\mathbf{x}}$ (a) and $\hat{\mathbf{y}}$ (b) directions respectively. (c,d) The same COM motion as (a,b) but for the complex system. Parameters are the same as that in (a,b) except that new terms C_3, C_4, C_5 are included in the condensate and COM motion caculations.
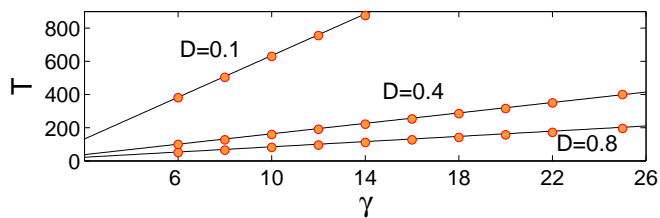
Figure 4: (Color online) Plot of the COM oscillation period T with respect to the SOC strength γ for the simple system in the TF phase. Circles are from the numerical stimulation of the G-P equation (3). The lines are from Eq. (5).

rections may be understood from the single atom dynamics with the Rashba SOC. The spin-orbit coupled atoms have two bands with energies $E_\pm = \hbar^2 k^2/2m \pm \gamma k$ and corresponding wavefunctions $\phi_\pm = \exp(i\mathbf{k} \cdot \mathbf{r})(1, \pm i e^{i\varphi_\mathbf{k}})^T/\sqrt{2}$, where $\varphi_\mathbf{k} = \arg(k_x + ik_y)$. The ground state of the atom ϕ_- stays at the potential minimum located at $k_0 = \gamma m/\hbar^2$ with the direction of $\mathbf{k}_0$ spontaneously selected. The shift of the harmonic trap corresponds to adding a momentum $\mathbf{p}$ into the ground state, leading to an initial state $\phi_{ini} = \exp(i\mathbf{p} \cdot \mathbf{r})\phi_-$. The time evolution of the wavefunction can be written as $\varphi(\mathbf{r}, t) = \int d\mathbf{k}[A_- \exp(iE_- t)\phi_- + A_+ \exp(iE_+ t)\phi_+]$, where $A_\pm = \langle\phi_\pm|\phi_{ini}\rangle$. When $\mathbf{p}$ is perpendicular to the direction of $\mathbf{k}_0$ (Fig. 2b), both $A_\pm$ are nonzero, and there is an interference between two spin-orbit coupled bands, leading to the SOC dependent oscillation of the COM motion (Fig. 3a). In contrast, when $\mathbf{p}$ is along the direction of $\mathbf{k}_0$, one of $A_\pm$ must be zero and there is only one oscillation frequency due to the harmonic trap.

We numerically calculate the new oscillation period T in Fig. 3a for several different sets of interaction parameters, and find that it does not depend on the interaction strengths C_1 and C_2, indicating essentially single particle physics in this system. In Fig. 4, we plot the dependence of T with respect to γ for three harmonic trap shifts D. The numerical data can be well fitted with an analytic formula

$$T = 2\pi(1 + \gamma/D). \tag{5}$$

We see that the period is linearly proportional to γ and D^{-1}. In the strong SOC region ($\gamma \gg 1$), the strong SOC couples many harmonic oscillator states and tends to reduce the single particle energy splitting, as confirmed by our numerical calculation, resulting in a large oscillation period. Note that this is very different from the ZB oscillation in the weak SOC region [9], where the oscillation period is proportional to γ^{-2} because the energy splitting between two spin-orbit coupled bands in this region is proportional to γ^2, as confirmed in our numerical simulation. Finally, a smaller shift D leads to less excitations to the high energy states, yielding a larger COM oscillation period. As $\gamma \to 0$, $T \to 2\pi$, the oscillation period for the harmonic trap frequency, as expected. In the weak

and medium interaction or SOC region, our numerical results show that the oscillation amplitude decays with time due to the phase separation of the densities of two pseudospin components (Figs. 2e-2h) that leads to the decoherence in the COM motion.

In the stripe phase of the simple system, the COM motion is always damped because of the decoherence originating from the spatial separation of two spin components. Similar as the TF phase, the new oscillation period disappears (emerges) when the shift is along (perpendicular to) the condensate phase variation direction.

The COM motion is strongly modified in the complex system. In Fig. 3c and 3d, we plot the COM motion in the TF phase. Clearly, the direction dependence of the new oscillation period is the same as that for the simple system. However, the oscillation period T is very different from that in the simple system (Fig. 3a) although the complex system has the same parameters (C_1, C_2, γ) as the simple one. A damping of the oscillation amplitude is also observed, in contrast to the perfect oscillation in the simple system. Furthermore, when the shift of the harmonic trap is along the condensate phase variation direction, the COM motion perpendicular to the shift direction emerges after a long time (Fig. 3d), in contrast to the zero motion in the simple system (Fig. 3b).

In experiments, we can choose the trapping frequency $\omega_\perp = 2\pi \times 20 Hz$, which yields the time unit $\omega_\perp^{-1} = 8ms$ and length unit $a_h = \sqrt{\hbar/m\omega_\perp} = 2.4 \mu m$. For Rb atoms, the spin-orbit coupling strength $\gamma \sim 1 - 10$. The interaction strength C_1, C_2 can be tuned through the Feshbach resonance or by adjusting the atom number. With $a_0, a_1 \sim 100a_B$ for Rb atoms, C_1, $C_2 \sim 10$ for $N \sim 300$, where $a_B = 0.53$ Å is the Bohr radius. We consider a multiple layer system generated by an optical lattice along the z direction, therefore the total number of atoms is $\sim 10^4$. We also confirm that the mean field dynamics are similar for larger interaction strength C_1, $C_2 \sim 100$, therefore the total number of atoms can be $\sim 10^5$. For an initial shift of the harmonic trap $D = 2$ and $\gamma = 6$, we find the center of mass oscillation period $T \sim 200$ ms, which is much shorter than the lifetime of the BEC and should be observable in experiments.

In summary, we derive a generic G-P equation and investigate the mean field dynamics for SOC-BECs. We emphasize that our G-P equation may serve as the starting point for the future study on the dynamics of SOC-BECs. Our predicted new oscillation period in the COM motion is observable in experiments and may provide a powerful tool for exploring the phase of the condensate wavefunction as well as the low energy excitations in SOC-BECs.

---

* Corresponding author, email:cwzhang@wsu.edu

[1] D. Xiao *et al.*, Rev. Mod. Phys. **82**, 1959 (2010).
[2] M. Z. Hasan, and C. L. Kane, Rev. Mod. Phys. **82**, 3045 (2010).
[3] I. Žutić *et al.*, Rev. Mod. Phys. **76**, 323 (2004).
[4] J. Ruseckas *et al.*, Phys. Rev. Lett. **95**, 010404 (2005).
[5] S.-L. Zhu *et al.*, Phys. Rev. Lett. **97**, 240401 (2006).
[6] X.-J. Liu *et al.*, Phys. Rev. Lett. **98**, 026602 (2007).
[7] T. D. Stanescu *et al.*, Phys. Rev. Lett. **99**, 110403 (2007).
[8] G. Juzeliūnas *et al.*, Phys. Rev. A **77**, 011802(R) (2008).
[9] J. Y. Vaishnav and C. W. Clark, Phys. Rev. Lett. **100**, 153002 (2008).
[10] T. D. Stanescu *et al.*, Phys. Rev. A **78**, 023616 (2008).
[11] C. Wu, and I. Mondragon-Shem, arXiv:0809.3532.
[12] C. Zhang *et al.*, Phys. Rev. Lett. **101**, 160401 (2008).
[13] X.-J. Liu *et al.*, Phys. Rev. Lett. **102**, 046402 (2009).
[14] I. B. Spielman, Phys. Rev. A **79**, 063613 (2009).
[15] Y.-J. Lin *et al.*, Nature **471**, 83 (2011).
[16] C. Zhang, Phys. Rev. A **82**, 021607(R) (2010).
[17] T.-L. Ho and S. Zhang, Phys. Rev. Lett. **107**, 150403 (2011).
[18] C. Wang *et al.*, Phys. Rev. Lett. **105**, 160403 (2010).
[19] M. Merkl *et al.*, Phys. Rev. Lett. **104**, 073603 (2010).
[20] J. Larson *et al.*, Phys. Rev. A **82**, 043620 (2010).
[21] B. T. Seaman *et al.*, Phys. Rev. A **75**, 023615 (2007).
[22] C. J. Pethick and H. Smith, *Bose-Einstein condensation in dilute gases* (2nd ed. Cambridge Press, 2008).
[23] For the laser setup in Fig. 1c [16], $d_1 = [\frac{1}{2} - i\frac{\sqrt{3}}{6}]e^{-ik\frac{\sqrt{3}x+y}{2}}$, $d_2 = -[\frac{1}{2} + i\frac{\sqrt{3}}{6}]e^{-ik\frac{\sqrt{3}x-y}{2}}$, $d_3 = i\frac{\sqrt{3}}{3}$, $f_1 = [-i\frac{1}{2}+\frac{\sqrt{3}}{6}]e^{-ik\frac{\sqrt{3}x+y}{2}}$, $f_2 = [i\frac{1}{2}+\frac{\sqrt{3}}{6}]e^{-ik\frac{\sqrt{3}x-y}{2}}$, $f_3 = -\frac{\sqrt{3}}{3}$. For the laser setup in Fig. 1d [8], $d_1 = [\frac{1}{2} - i(\frac{1}{\sqrt{2}} - \frac{1}{2})]e^{-ik(x+y)}$, $d_2 = -[\frac{1}{2}+i(\frac{1}{\sqrt{2}}-\frac{1}{2})]e^{-ik(x-y)}$, $d_3 = i\sqrt{\sqrt{2}-1}$, $f_1 = -i[\frac{1}{2}+i(\frac{1}{\sqrt{2}}-\frac{1}{2})]e^{-ik(x+y)}$, $f_2 = i[\frac{1}{2} - i(\frac{1}{\sqrt{2}} - \frac{1}{2})]e^{-ik(x-y)}$, $f_3 = -\sqrt{\sqrt{2}-1}$.
[24] The nonlinear coefficients $C_1 = 2N\sum_{\alpha,\beta=1}^{3} g_{\alpha\beta}|d_\alpha|^2|d_\beta|^2$, $C_2 = 2N\sum_{\alpha,\beta=1}^{3} g_{\alpha\beta}\left(|d_\alpha|^2|f_\beta|^2 + d_\alpha^* f_\alpha d_\beta f_\beta^*\right)$, $C_3 = 2N\sum_{\alpha,\beta=1}^{3} g_{\alpha\beta}|d_\alpha|^2 d_\beta^* f_\beta$, $C_4 = 2N\sum_{\alpha,\beta=1}^{3} g_{\alpha\beta}|f_\alpha|^2 d_\beta^* f_\beta$, $C_5 = 2N\sum_{\alpha,\beta=1}^{3} g_{\alpha\beta} d_\alpha^* f_\alpha d_\beta^* f_\beta$, and $C_6 = 2N\sum_{\alpha,\beta=1}^{3} g_{\alpha\beta}|f_\alpha|^2|f_\beta|^2$.
[25] D. L. Campbell, G. Juzelinūas, I. B. Spielman, arXiv:1102.3945.
[26] S. Stringari, Phys. Rev. Lett. **77**, 2360 (1996).